On the sound wave attenuation by spatiotemporally reconfigurable grating

A. Berezovski

Tallinn University of Technology, School of Sciences, Tallinn, Estonia

ARTICLE HISTORY
Compiled September 4, 2025

ABSTRACT
Controllable wave propagation is impossible when the properties of a material or structure are fixed by fabrication. External actions are inevitable for adjusting material properties to change wave field characteristics in a desirable way. Another way to manage the wave field is to reconfigure the inner structure. This approach is exemplified in the paper by analyzing wave propagation through a space-time reconfigurable diffraction grating in air. The diffraction grating can be dynamically adjusted by moving it back and forth, creating a time-periodic change in its configuration. Instantaneous space-time reconfiguration represents the limit case for wave propagation control. It is demonstrated that in this limit scenario, complete sound isolation is achievable.

KEYWORDS
Diffraction grating; wave propagation; numerical simulation, dynamic device

1. Introduction

The objective of the paper is to examine sound wave propagation through a rigid diffraction grating with time-dependent reconfiguration. A reconfigurable diffraction grating that alters the location of an internal composition in space and time is an example of an active metamaterial. Active metamaterials are structures that incorporate both inhomogeneous material and means of varying its properties or/and configurations [1–4]. Material cannot change its properties on its own within a short period of time. External stimuli are required for their characteristics to be time-varying [5–7]. The use of materials that vary in space and time is the focus of contemporary wave control studies [1, 8, 9].

Analytical study of the electromagnetic wave diffraction from space-time-periodic gratings and shows "that such gratings provide an infinite number of spatial diffraction orders, each of which is composed of an infinite number of temporal diffraction orders" [10]. It is essential that space-time-periodic gratings represent the periodic change of material properties without changing the grating's geometry [10]. In contrast, a spatiotemporally reconfigurable grating changes the positions of grating elements without modifying their material properties. The reconfigurability of the diffraction grating does not reduce to the modulation in time as presented in [11] because there is no single moving frame. It seems that direct numerical simulation of the wave propagation

CONTACT A. Berezovski. Email: arkadi.berezovski@taltech.ee

problem is the most practical method for evaluating the integrated effect of reconfigurability on sound wave attenuation by spatiotemporally reconfigurable gratings.

Wave propagation through diffraction gratings has been studied for a long time. In 1836, Henry Fox Talbot observed the self-imaging effect caused by the interference of incident plane light waves propagating through a periodic structure. Later on, this effect was named after him. The Talbot effect was explained theoretically by Lord Rayleigh in 1881. The Talbot effect has been observed not only in optics [12–14], but also in acoustics [15], ultrasonics [16], and elasticity [17]. Wave propagation through diffraction gratings is closely related to a more general problem of wave propagation across a rigid microstructure. The corresponding initial value problem appears to be unsolvable directly [18]. Numerical simulations of such problems use homogenized models of gratings [19–22]. However, the self-imaging Talbot effect cannot be reproduced using the homogenization approach [19–22].

This is another reason to conduct a direct numerical simulation (without homogenization) of wave propagation through a reconfigurable diffraction grating to observe how spatial and temporal variability affects the sound wave behavior.

The structure of the paper is as follows. First, sound wave diffraction by a conventional stationary rigid grating is investigated. Calculations reveal the grating's self-imaging effect as well as the frequency dependence of sound transmission. Next, the reconfiguration of the grating caused by its back and forth motion with finite velocity is examined. As a result, the wave field becomes distorted, and the sound attenuation increases. Finally, we look at the limit case in which the grating location changes instantly. Numerical simulations show that instant periodic changing the location of the grating can result in complete sound reflection if the period of change is sufficiently short.

2. Wave propagation through diffraction grating

A diffraction grating is a structure made up of a periodic row of embedded inclusions in a material. The properties of inclusions differ from those of the surrounding material. A two-dimensional illustration of a diffraction grating is shown in Fig. 1.

We are dealing with a grating composed of rigid inclusions in air. To visualize the sound wave field behind the grating, the numerical solution to linearized acoustic equations

$$\frac{\partial p}{\partial t} + \rho c^2 \, div \, \mathbf{v} = 0, \tag{1}$$

$$\frac{\partial \mathbf{v}}{\partial t} + \frac{1}{\rho} \, grad \, p = 0, \tag{2}$$

is performed. These equations can be reduced to the wave equation of sound pressure p

$$\frac{\partial^2 p}{\partial t^2} - c^2 \nabla^2 p = 0, \tag{3}$$

Here ρ is the matter density, c is the speed of sound, and $\mathbf{v}$ is the particle velocity

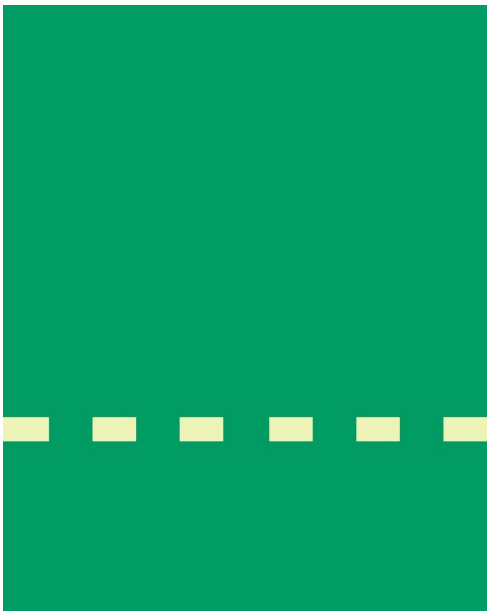

Figure 1. Diffraction grating sketch.

vector.

2.1. Time-harmonic wave

For a time-harmonic wave in two space dimensions

$$p = \hat{p}(x, y)e^{i\omega t}, \tag{4}$$

we can rewrite Eq. (3) as

$$-\omega^2\hat{p} - c^2\left(\frac{\partial^2\hat{p}}{\partial x^2} + \frac{\partial^2\hat{p}}{\partial y^2}\right) = 0. \tag{5}$$

Performing a dimensional analysis will reveal the governing parameters of the problem. Let each inclusion have a horizontal size a equal to the distance between them. The vertical inclusion length is denoted as l, while the characteristic frequency of the process is ω_0. Introducing dimensionless variables

$$X = \frac{x}{a}, \quad Y = \frac{y}{l}, \quad \overline{\omega} = \frac{\omega}{\omega_0}, \tag{6}$$

we can represent Eq. (5) in terms of dimensionless variables

$$\omega_0^2\overline{\omega}^2\hat{p} + c^2\left(\frac{\partial^2\hat{p}}{a^2\partial X^2} + \frac{\partial^2\hat{p}}{l^2\partial Y^2}\right) = 0. \tag{7}$$

The characteristic frequency is chosen as

$$\omega_0 = c/\lambda, \tag{8}$$

where λ is the length of the incoming harmonic wave. Then the dimensionless wave equation (7) is represented as follows:

$$\frac{1}{\lambda^2}\overline{\omega}^2\hat{p} + \frac{1}{a^2}\left(\frac{\partial^2\hat{p}}{\partial X^2} + \frac{a^2\partial^2\hat{p}}{l^2\partial Y^2}\right) = 0. \tag{9}$$

It is worth noting that if $l \gg a$, the second term in parenthesis can be neglected. This means that sound pressure will be independent of the vertical coordinate y. Accordingly, if, *vice versa*, $a \gg l$, then sound pressure will be independent of the horizontal coordinate x. It is not feasible to use either limit case. As a result, we restrict ourselves to inclusions with comparable vertical and horizontal sizes.

The geometry of grating elements and their arrangement offer limitless opportunities for creating diverse situations. To see how the reconfigurability affects the sound wave attenuation, it is therefore helpful to select a simple configuration. In the *reference* scenario of square grating elements (with the choice $a = l$) we arrive at the dimensionless equation

$$\overline{\omega}^2\hat{p} + \frac{\lambda^2}{a^2}\left(\frac{\partial^2\hat{p}}{\partial X^2} + \frac{\partial^2\hat{p}}{\partial Y^2}\right) = 0. \tag{10}$$

Thus, the governing parameter of the reference scenario is the ratio of the incoming wavelength λ and the size of inclusions a (with the characteristic frequency $\omega_0 = c/\lambda$).

2.2. Stationary grating

First, we consider wave propagation across the conventional stationary grating. Without loss of generality, we choose grating elements that are 20 space steps in size. The wave equation (10) is solved in a two-dimensional computational domain with size 220×500 space steps. The square rigid grating is placed at the distance between 140 and 160 space steps from the bottom. A time-harmonic sound wave generated at the bottom boundary has the amplitude normalized to 100 units. The upper boundary is pressure-free. Periodicity conditions at the lateral boundaries are used to maintain plane wave propagation. The numerical solution to wave equation (10) was performed with the thermodynamically consistent version of the finite-volume wave propagation algorithm [23]. In this version, each computational cell is handled as a discrete thermodynamic system according to [24]. Averaged field quantities describe the local equilibrium state of each cell. Jump relations at computational cell boundaries represent the continuity of actual values and are used to exactly determine numerical fluxes [23]. After that, transversal fluxes are calculated [25]. As a result, an explicit conservative, high-order accurate wave propagation algorithm is created. Standard boundary conditions are applied using ghost cells [25]. At every interface, wave transmission and reflection are managed automatically, accounting for any discontinuities in the parameters. This is the primary advantage of the finite volume wave propagation algorithm [25]. The selection of space and time steps provides the Courant number of one. This is upper limit of stability of the applied numerical scheme which provides exact solution to the problem in one dimension [25].

Calculations of the wave propagation across the diffraction grating were carried out over 1000 time steps. The computed distribution of the sound pressure exhibits the Talbot effect. The Talbot effect manifests itself in the appearance of the so-called Talbot carpet as a result of the interference of transmitted waves, as illustrated in

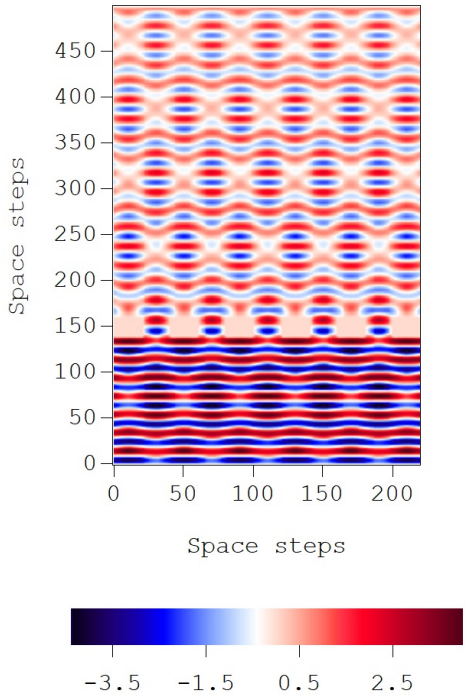

Figure 2. Contour plot of the sound pressure at 1000 time steps in the case of stationary grating.

Fig. 2. The Talbot carpet in this figure corresponds to the incident sound wavelength, which is equal to the size of the grating elements as in the reference scenario. The Talbot carpet exhibits a consistent self-imaging pattern of the wave field behind the stationary grating [12].

In turn, the surface plot of the sound pressure (Fig. 3) demonstrates that the diffraction of the sound wave by the grating causes sound attenuation. The measure of the attenuation is the transmission loss (in decibels (dB)) determined by the ratio of the incident sound intensity I_{inc} and the transmitted sound intensity I_{trans} [26, 27]

$$STL = 10 \lg \frac{I_{inc}}{I_{trans}}. \tag{11}$$

The sound intensity is proportional to the square of the sound pressure [26, 27]. The sound pressure behind the diffraction grating was computed for a variety of incoming wavelengths. Then the values of sound transmission loss were determined. The calculated spectrum of the sound transmission loss for the stationary diffraction grating is represented in Fig. 4 by red curve. It illustrates the frequency-dependent nature of sound transmission through the stationary grating. As can be seen, maximum sound transmission occurs at small wavelengths that are comparable in size to the grating elements. This correlates with experimental observations [28, 29].

Numerical simulations of sound wave propagation across rigid stationary gratings reveal the well-known Talbot effect. This indicates that the finite volume numerical technique is an appropriate choice for solving the wave propagation problem as it has been formulated.

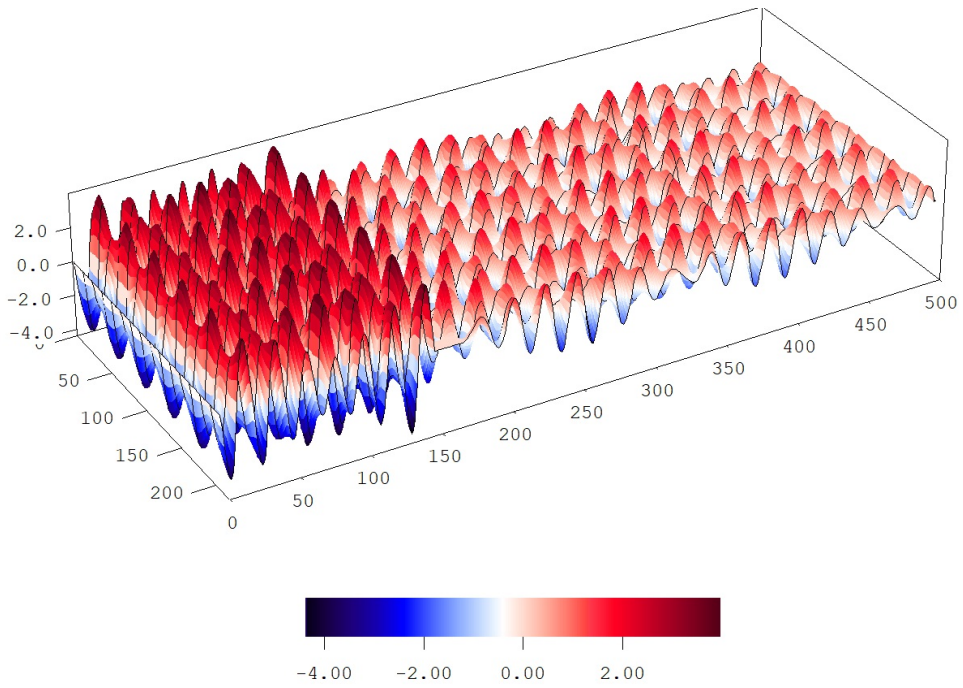

Figure 3. Surface plot of the sound pressure at 1000 time steps in the case of stationary grating.

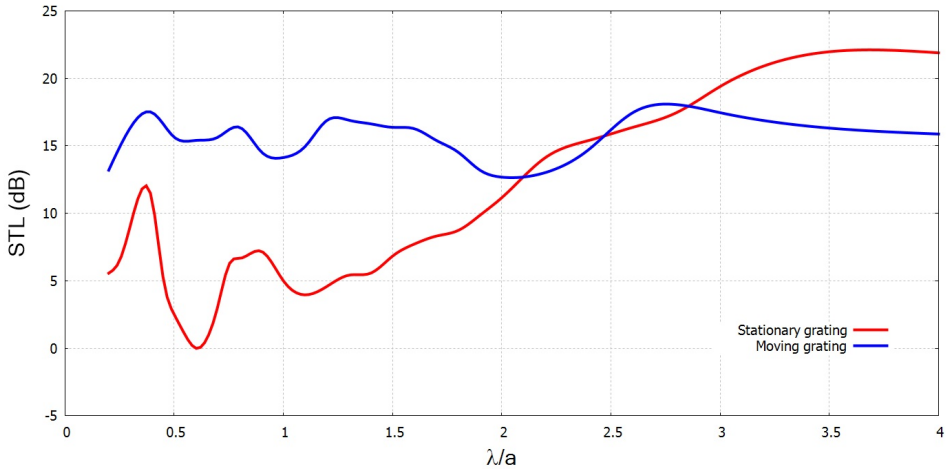

Figure 4. Sound transmission loss *vs* dimensionless wavelength. Red curve corresponds to the stationary grating. Blue curve represents the transmission spectrum of the reconfigurable grating.

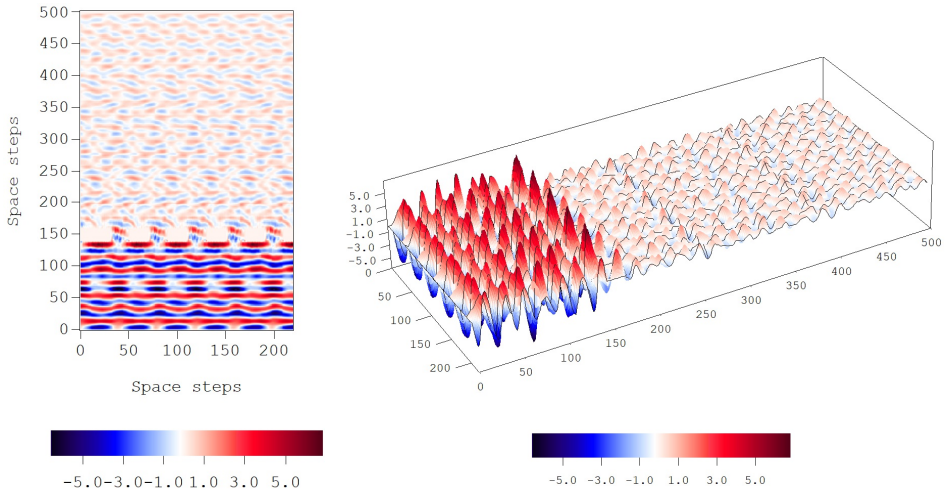

Figure 5. Sound pressure distribution at 1000 time steps in the case of reconfigurable grating moving back and forth with velocity $v = 0.25c$. Left panel - contour plot; right panel - surface plot.

3. Space-time grating reconfiguration

Now we examine what happens if the grating is reconfigurable in space and time. The considered reconfiguration suggests that the grating moves along its axis with a velocity v for a set amount of time and then returns to its original position with the same velocity. This indicates that the grating's spatial periodicity is supplemented by its temporal periodicity. We employ the same numerical algorithm as before because of its robustness.

The grating may be reconfigured at a variety of its speeds. A number of simulations were carried out in order to investigate how the reconfiguration velocity affected the propagation of plane harmonic sound waves through reconfigurating gratings. A few examples of calculation results are presented in the form of sound pressure distributions at the specified time instant below. The sound pressure distribution corresponding to the velocity of the grating reconfiguration $v = 0.25c$ is presented in Fig. 5. The contour plot of the sound pressure (Fig. 5a) shows that the sound wave field is distorted as the grating moves back and forth. The surface plot (Fig. 5b) demonstrates that sound attenuation is increased compared to a stationary grating case.

Similar calculations were performed for the grating reconfiguration velocity $v = 0.5c$. Results for the sound pressure distribution in this case are given in Fig. 6. The faster grating reconfiguration increases both sound attenuation (Fig. 6b) and sound field distortion (Fig. 6a).

Calculations of the sound wave propagation through reconfigurable grating with velocity $v = 0.75c$ were also conducted for the comparison (see Fig. 7). Results of numerical calculations presented in Fig. 7 confirm that the wave field becomes more distorted as the grating reconfiguration velocity increases. Additionally, reconfiguration of the grating reduces sound transmission when compared to the stationary grating case. This is illustrated in Fig. 4, where the blue line represents the transmission spectrum of the reconfigurable grating. In the given case, the velocity of the grating motion is the same as the sound speed in air.

According to numerical simulations, sound transmission through the reconfigurable grating tends to decrease as the reconfiguration velocity increases. The dependence

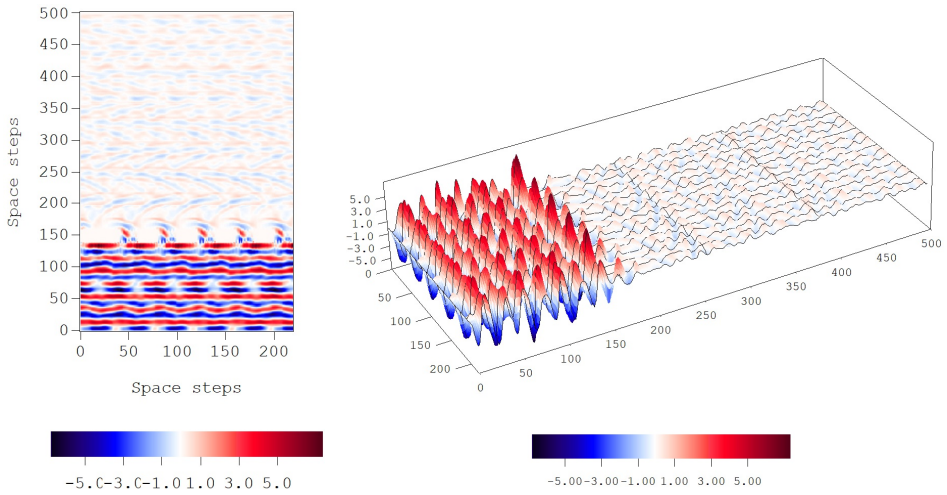

Figure 6. Sound pressure distribution at 1000 time steps in the case of reconfigurable grating moving back and forth with velocity $v = 0.5c$. Left panel - contour plot; right panel - surface plot.

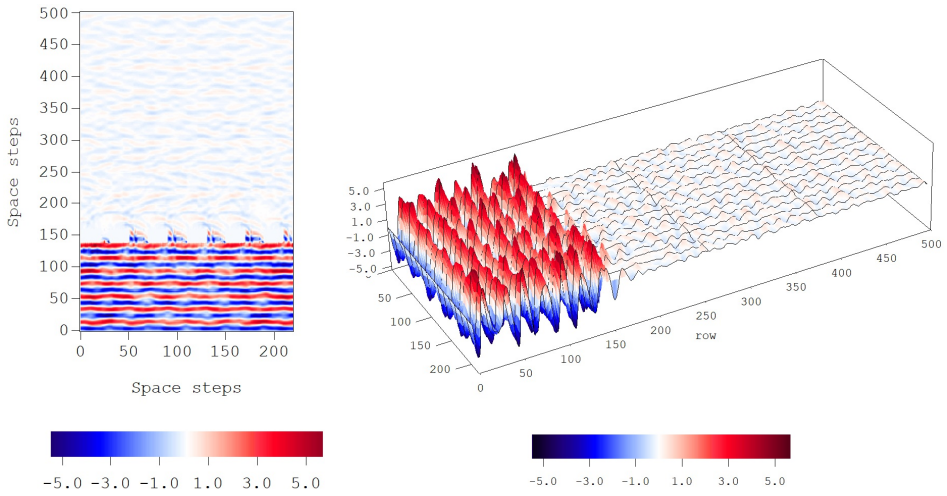

Figure 7. Sound pressure distribution at 1000 time steps in the case of reconfigurable grating moving back and forth with velocity $v = 0.75c$. Left panel - contour plot; right panel - surface plot.

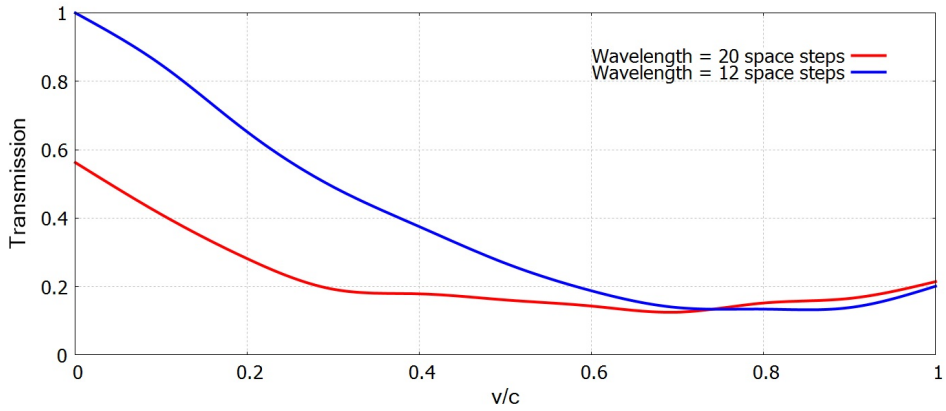

Figure 8. Sound transmission dependence on the reconfiguration velocity.

of sound transmission on the reconfiguration velocity is illustrated in Fig. 8. The red curve corresponds to the incoming wavelength equal to the size of the grating cell a, while the blue curve represents the results for the wavelength of $0.6a$ which corresponds to the minimal sound transmission loss for stationary grating (Fig. 4).

Although the tendency of sound transmission to decrease with increasing grating reconfiguration velocity is not entirely straight, it does suggest that further velocity increase may produce unexpected results. The limit case in which the grating motion's velocity is infinite corresponds to instantaneous reconfiguration.

4. Instantaneous reconfiguration

The instantaneous altering of configuration of inclusions in space and time is idealized in the theory of so-called dynamic materials [30, 31]. Introduced in the late 1990s, the notion of dynamic materials was further refined in [32–34]. Such an idealization results in unusual wave patterns even in a one-dimensional setting [35–37].

In the idealized scenario, the grating switches to an alternate position (shifted by 20 space steps) every 20 time steps instantaneously. We refer to this type of reconfiguration as dynamic reconfiguration. The time variation of the grating location in the case of dynamic reconfiguration is shown in Fig. 9. Discontinuous boundary conditions emerge at the grating elements when the grating's position changes instantly. Nevertheless, numerical simulations of the harmonic plane sound wave propagation can be performed as before due to the robustness of the finite volume algorithm.

The obtained sound pressure distribution at 1000 time steps is presented in Fig. 10. The wavelength of the incoming wave in this case is equal to the size of grating elements. It is fascinating that no sound can penetrate through the rigid, dynamically space-time-reconfiguring grating. This is achievable if the frequency of the incoming wave used falls within a stop band. Examining different frequency values is necessary to establish the stop band's limits. Number of calculations for certain arbitrarily selected frequencies consistently lead to the complete absence of sound behind the dynamically spatiotemporally reconfigurable grating.

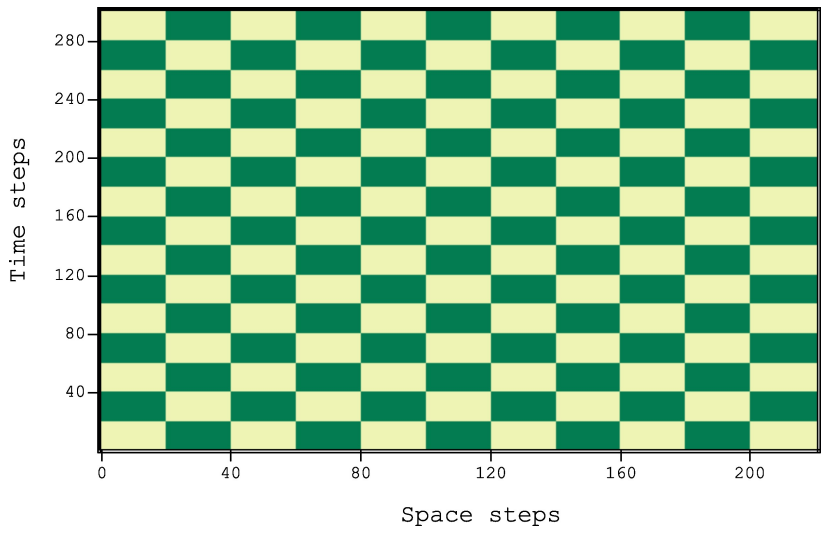

Figure 9. Dynamic space-time variation of the grating.

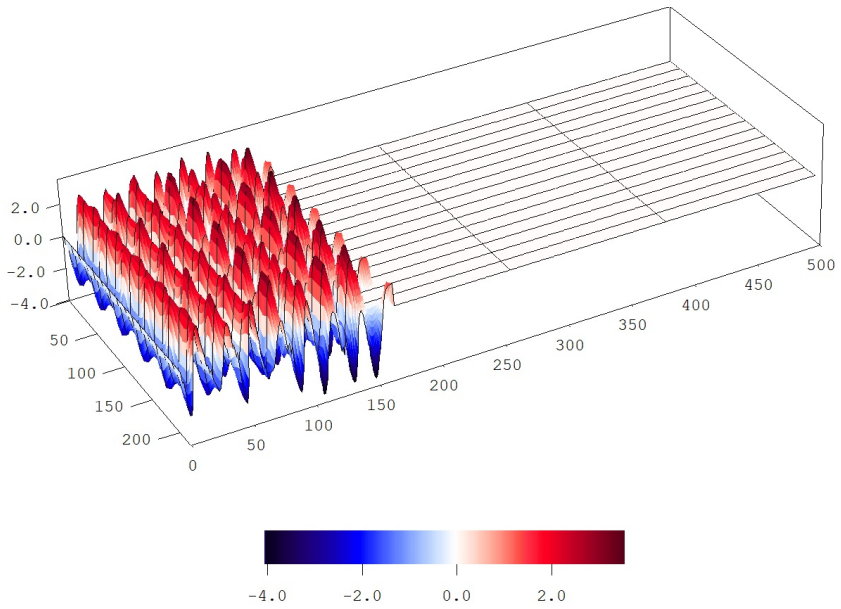

Figure 10. Surface plot of the sound pressure distribution at 1000 time steps in the case of dynamically reconfigurable diffraction grating.

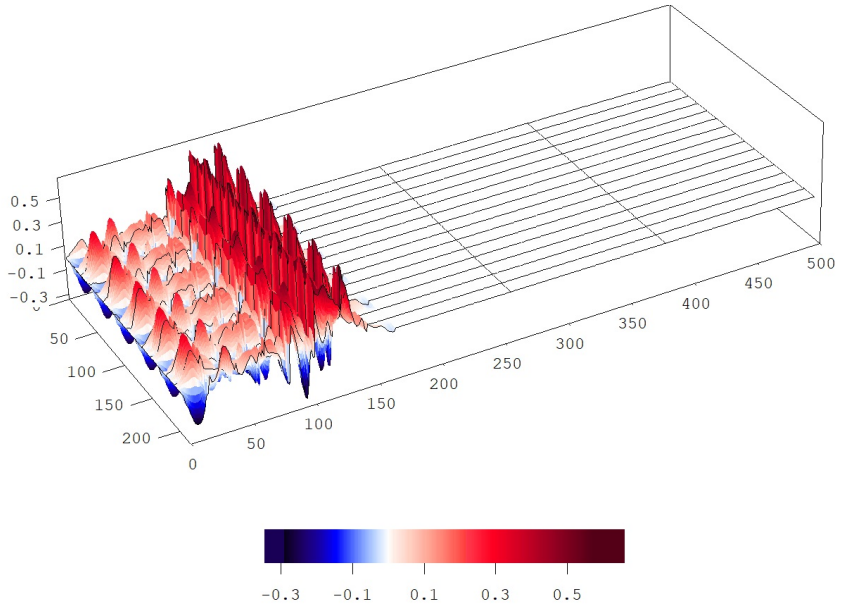

Figure 11. Surface plot of the sound pressure distribution at 1000 time steps in the case of pulse propagation. Width of the incoming pulse is equal to 100 space steps.

4.1. Pulse propagation

To ensure that the rigid grating dynamically reconfigurable in space and time provides sound insulation, we examine the pulse propagation scenario, because pulse contains an infinite number of frequencies. A finite-duration smooth pulse is generated at the bottom boundary. The pulse amplitude changes according to the expression

$$\hat{p} = sin^2(\pi t/d), \quad \text{for} \quad t < d\Delta t, \tag{12}$$

where d is the width of the pulse measured in space steps. Once the generation is complete, the bottom boundary is pressure-free.

Figure 11 shows the example of sound pulse propagation calculations. The pulse duration there corresponds to 100 time steps. The amplitude of the finite pulse is determined by the total energy it contains. As can be seen, the sound pressure is zero behind the dynamically reconfigurable rigid grating embedded in air. Repeated sound field calculations for pulses of various shapes and durations yield the same results. This verifies that, for the selected geometry and time period of alteration, no sound is transmitted through the dynamically changing rigid grating for all frequencies. The dynamically reconfigurable rigid grating is therefore a perfect candidate for a sound isolation device, at least theoretically.

4.2. Variation in the alteration period

Let's examine what happens when we change the interval between grating alterations over time. Fixing the dimensionless frequency of the incoming harmonic sound wave at $\overline{\omega} = 2$, we calculated the sound wave field for different alteration intervals. The results of our calculations for alteration periods of 10, 20, 40, and 80 time steps, showing the sound pressure distribution along the centerline of the computational domain, are

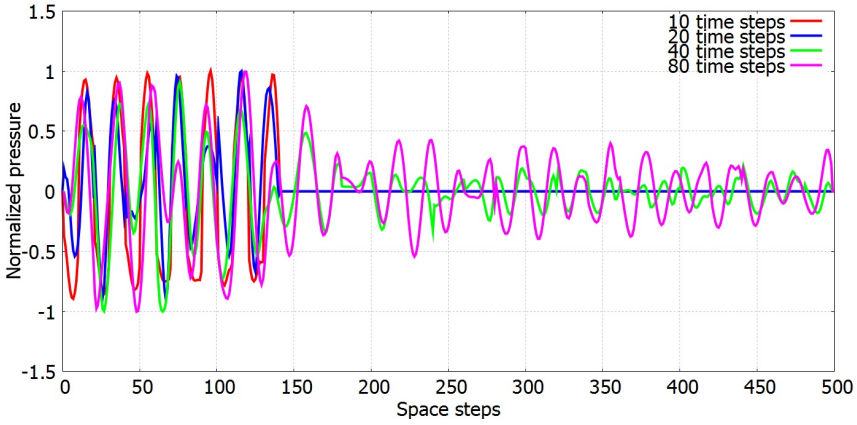

Figure 12. Sound pressure distribution along centerline at 1000 time steps for different alteration periods.

presented in Fig. 12.

It is readily apparent that sound isolation only emerges with short periods of grating alteration (red and blue curves in Fig. 12). If the grating alteration is prolonged, the sound isolation fails. This is expected because the gradual change of the grating approaches its stationary state.

5. Discussion

Transmissive diffraction gratings can be considered as components of periodic scatterer arrays, which are widely used for sound reduction and noise barriers [38–43]. Stationary diffraction gratings offer the simplest geometry available for theoretical analysis [28, 44–46]. It has been shown that the transmission of sound across an stationary diffraction grating can be adjusted by varying geometry and periodicity of the grating elements [46]. Limitless situations can be created based on geometry and material variation rules. Once manufactured, stationary diffraction gratings have a fixed and narrow working band [47].

New and promising opportunities for noise reduction and sound attenuation are provided by active metamaterials [7]. These materials have the ability to change their properties in both space and time under external stimuli [1, 8, 48]. However, as it was noted, "little progress has been made in the implementation of acoustic metamaterial-based noise barriers for real applications in the past few years" [49].

Reconfigurable diffraction gratings that change the position of their elements in space and over time while preserving their material properties can offer novel possibilities to control sound waves. A diffraction grating can be reconfigured by moving it back and forth. Rotation of rigid square rod scatterers may also allow space-time variation of a grating [50, 51].

6. Conclusion

The paper presents a numerical investigation of sound wave propagation and attenuation through diffraction gratings under various diffraction grating reconfiguration scenarios. Numerical simulations of sound wave propagation are performed in two-

dimensional setting. The linear acoustics equations are solved using a thermodynamically consistent and second-order accurate finite-volume numerical technique. The acoustical Talbot effect is shown in the case of a rigid stationary diffraction grating, confirming the suitability of the numerical algorithm.

The reconfiguration suggests that the grating moves back and forth along its axis providing temporal periodicity of the problem. A number of simulations were carried out in order to study how the reconfiguration velocity affected the propagation of plane harmonic sound waves through gratings. It is shown that the back and forth motion of the grating reduces sound transmission across it when compared to a stationary grating.

It is demonstrated that total sound isolation can be accomplished in the idealized scenario by instantaneously altering the location of the grating elements. The sound isolation in this case is independent of frequency. However, the sound isolation only emerges with short periods of grating alteration.

Funding

This research was supported by the Estonian Research Council under Research Project RPG1227.

References

[1] Chen S, Fan Y, Fu Q, et al. A review of tunable acoustic metamaterials. Applied Sciences. 2018;8(9):1480.
[2] Zangeneh-Nejad F, Fleury R. Active times for acoustic metamaterials. Reviews in Physics. 2019;4:100031.
[3] Kumar S, Pueh Lee H. Recent advances in active acoustic metamaterials. International Journal of Applied Mechanics. 2019;11(08):1950081.
[4] Gao N, Zhang Z, Deng J, et al. Acoustic metamaterials for noise reduction: a review. Advanced Materials Technologies. 2022;7(6):2100698.
[5] Yi K, Ouisse M, Sadoulet-Reboul E, et al. Active metamaterials with broadband controllable stiffness for tunable band gaps and non-reciprocal wave propagation. Smart Materials and Structures. 2019;28(6):065025.
[6] Wang YF, Wang YZ, Wu B, et al. Tunable and active phononic crystals and metamaterials. Applied Mechanics Reviews. 2020;72(4):040801.
[7] Ji G, Huber J. Recent progress in acoustic metamaterials and active piezoelectric acoustic metamaterials - A review. Applied Materials Today. 2022;26:101260.
[8] Popa BI, Zigoneanu L, Cummer SA. Tunable active acoustic metamaterials. Physical Review B. 2013;88:024303.
[9] Qi J, Chen Z, Jiang P, et al. Recent progress in active mechanical metamaterials and construction principles. Advanced Science. 2022;9(1):2102662.
[10] Taravati S, Eleftheriades GV. Generalized space-time-periodic diffraction gratings: Theory and applications. Physical Review Applied. 2019;12(2):024026.
[11] Pham K, Maurel A. Diffraction grating with space-time modulation. Journal of Computational Physics. 2022;469:111528.
[12] Patorski K. The self-imaging phenomenon and its applications. Progress in Optics, Elsevier; 1989. p. 1–108.
[13] Berry MV, Klein S. Integer, fractional and fractal Talbot effects. Journal of Modern Optics. 1996;43(10):2139–2164.

[14] Wen J, Zhang Y, Xiao M. The Talbot effect: recent advances in classical optics, nonlinear optics, and quantum optics. Advances in Optics and Photonics. 2013;5(1):83–130.
[15] Fisicaro M, Doedes Y, Steenbergen T, et al. Observation of the talbot effect from a surface-acoustic-wave dynamic grating. Physical Review A. 2025;111(4):043513.
[16] Candelas P, Fuster JM, Pérez-López S, et al. Observation of ultrasonic Talbot effect in perforated plates. Ultrasonics. 2019;94:281–284.
[17] Berezovski A, Engelbrecht J, Berezovski M. Pattern formation of elastic waves and energy localization due to elastic gratings. International Journal of Mechanical Sciences. 2015; 101-102:137–144.
[18] Maurel A, Mercier JF, Félix S. Wave propagation through penetrable scatterers in a waveguide and through a penetrable grating. The Journal of the Acoustical Society of America. 2014;135(1):165–174.
[19] Maurel A, Félix S, Mercier JF. Enhanced transmission through gratings: Structural and geometrical effects. Physical Review B. 2013;88(11).
[20] Lombard B, Maurel A, Marigo JJ. Numerical modeling of the acoustic wave propagation across a homogenized rigid microstructure in the time domain. Journal of Computational Physics. 2017;335:558–577.
[21] Touboul M, Pham K, Maurel A, et al. Effective resonant model and simulations in the time-domain of wave scattering from a periodic row of highly-contrasted inclusions. Journal of Elasticity. 2020;142(1):53–82.
[22] Pham K, Lebbe N, Maurel A. Diffraction grating with varying slit width: Quasi-periodic homogenization and its numerical implementation. Journal of Computational Physics. 2023;473:111727.
[23] Berezovski A, Engelbrecht J, Maugin GA. Numerical simulation of waves and fronts in inhomogeneous solids. World Scientific Publishing Co. Pte. Ltd.; 2008.
[24] Muschik W, Berezovski A. Thermodynamic interaction between two discrete systems in non-equilibrium. Journal of Non-Equilibrium Thermodynamics. 2004;29(3):237–255.
[25] LeVeque RJ. Finite volume methods for hyperbolic problems. Cambridge University Press; 2002.
[26] Raichel DR. The science and applications of acoustics. Springer Science & Business Media; 2006.
[27] Kuttruff H. Acoustics: an introduction. CRC Press; 2007.
[28] Lu MH, Liu XK, Feng L, et al. Extraordinary acoustic transmission through a 1D grating with very narrow apertures. Physical Review Letters. 2007;99(17):174301.
[29] Qi DX, Fan RH, Peng RW, et al. Multiple-band transmission of acoustic wave through metallic gratings. Applied Physics Letters. 2012;101(6):061912.
[30] Lurie KA. Effective properties of smart elastic laminates and the screening phenomenon. International Journal of Solids and Structures. 1997;34(13):1633–1643.
[31] Blekhman II, Lurie KA. On dynamic materials. Doklady Physics. 2000;45(3):118–121.
[32] Lurie KA. An introduction to the mathematical theory of dynamic materials. Springer; 2017.
[33] Rousseau M, Maugin GA, Berezovski M. Elements of study on dynamic materials. Archive of Applied Mechanics. 2011;81:925–942.
[34] Berezovski M, Berezovski A. Numerical simulation of energy localization in dynamic materials. Advances in Mechanics of Microstructured Media and Structures, Springer International Publishing; 2018. p. 75–83.
[35] Milton GW, Mattei O. Field patterns: a new mathematical object. Proceedings of the Royal Society A: Mathematical, Physical and Engineering Sciences. 2017; 473(2198):20160819.
[36] Mattei O, Milton GW. Field patterns without blow up. New Journal of Physics. 2017; 19(9):093022.
[37] Mattei O, Gulizzi V. On the effects of suitably designed space microstructures in the propagation of waves in time modulated composites. Applied Physics Letters. 2023; 122(6):061701.

[38] Sanchez-Perez JV, Rubio C, Martinez-Sala R, et al. Acoustic barriers based on periodic arrays of scatterers. Applied Physics Letters. 2002;81(27):5240–5242.
[39] Morandi F, Miniaci M, Marzani A, et al. Standardised acoustic characterisation of sonic crystals noise barriers: Sound insulation and reflection properties. Applied Acoustics. 2016;114:294–306.
[40] Fredianelli L, Del Pizzo LG, Licitra G. Recent developments in sonic crystals as barriers for road traffic noise mitigation. Environments. 2019;6(2).
[41] Iannace G, Ciaburro G, Trematerra A. Metamaterials acoustic barrier. Applied Acoustics. 2021;181:108172.
[42] Qin X, Ni A, Chen Z, et al. Numerical modeling and field test of sonic crystal acoustic barriers. Environmental Science and Pollution Research. 2023;30(6):16289–16304.
[43] Mohapatra K, Jena D. Numerical and experimental methods to measure the acoustic performance of sonic crystal noise barrier. Building Acoustics. 2023;30(3):339–356.
[44] Zhang X. Acoustic resonant transmission through acoustic gratings with very narrow slits: Multiple-scattering numerical simulations. Physical Review B. 2005;71(24):241102(R).
[45] Norris AN, Su X. Enhanced acoustic transmission through a slanted grating. Comptes Rendus Mécanique. 2015;343(12):622–634.
[46] Yu X, Lu Z, Liu T, et al. Sound transmission through a periodic acoustic metamaterial grating. Journal of Sound and Vibration. 2019;449:140–156.
[47] Mir F, Mandal D, Banerjee S. Metamaterials for acoustic noise filtering and energy harvesting. Sensors. 2023;23(9):4227.
[48] Cummer SA, Christensen J, Alù A. Controlling sound with acoustic metamaterials. Nature Reviews Materials. 2016;1(3):1–13.
[49] Kumar S, Lee HP. The present and future role of acoustic metamaterials for architectural and urban noise mitigations. Acoustics. 2019;1(3):590–607.
[50] Goffaux C, Vigneron J. Theoretical study of a tunable phononic band gap system. Physical Review B. 2001;64(7):075118.
[51] Romero-García V, Lagarrigue C, Groby J, et al. Tunable acoustic waveguides in periodic arrays made of rigid square-rod scatterers: theory and experimental realization. Journal of Physics D: Applied Physics. 2013;46(30):305108.